A NEW MODEL OF IRON OXIDE NANOPARTICLE MAGNETIC PROPERTIES TO GUIDE DESIGN OF NOVEL NANOMATERIALS

By

Ryan Adam Ortega

Thesis

Submitted to the Faculty of the

Graduate School of Vanderbilt University

in partial fulfillment of the requirements

for the degree of

MASTER OF SCIENCE

in

Biomedical Engineering

December, 2010

Nashville, Tennessee

Approved:

Professor Todd D. Giorgio

Professor H. Charles Manning

I would like to dedicate this work to my friends and family:

Thanks for being interested in my work,

even when you had no clue what I was talking about

ACKNOWLEDGEMENTS

This work was made possible in part by a grant from the United States Department of Defense's (USDoD) Congressionally Directed Medical Research Programs (CDMRP) Breast Cancer Research Program (BCRP): Grant BC076499. I would especially like to thank my advisor, Dr. Todd Giorgio for his guidance and direction regarding both the science presented in this work and the course of my present and future career. I would also like to thank my labmates, Shann Yu and Charleson Bell, for their scientific discussion and input, as well as their moral support, over the course of this project.

TABLE OF CONTENTS

Page

DEDICATION ii

ACKNOWLEDGEMENTS iii

LIST OF TABLES v

LIST OF FIGURES vi

LIST OF ABBREVIATIONS vii

Chapter

I. INTRODUCTION 1

Laboratory and clinical uses of iron oxide nanoparticles 2
Some laboratory uses of small magnetic particles 2
Some clinical uses of SPIONs 3
Activatable MRI contrast agents 5
An engineering model as a tool for material design 6

II. A MATHEMATICAL MODEL OF THE MAGNETIC PROPERTIES OF SUPERPARAMAGNETIC IRON OXIDE NANOPARTICLES 7

Assumptions and initializing parameters 7
Determining the magnetization of an individual particle 10
Graphing the magnetic field of a SPION 14

III. RESULTS AND IMPLICATIONS OF THE MODEL 17

Magnetization trends 17
Predicting linearity of magnetic behavior 20

IV. USING THE MODEL TO DESIGN NOVEL NANOMATERIALS: A 2D EXTRAPOLATION OF A CLUSTERED PARTICLE SYSTEM 23

Preliminary steps for model utilization:
a priori knowledge of desired SPION activity 23
Geometric considerations for 2D cluster modeling 24
Estimation of ideal particle size 28

V. CONCLUSIONS AND FUTURE WORK 33

BIBLIOGRAPHY 34

LIST OF TABLES

Table Page

1. Initializing assumptions for the model of SPION magnetization 10

LIST OF FIGURES

Figure		Page
1.	A model of an individual SPION and clustered SPIONs	9
2.	The vector magnetic field from a 20 nm SPION in a 1 T applied field	15
3.	The magnitude of the magnetic field from a SPION along a single radial line	16
4.	The saturation magnetization of SPIONs differs from the bulk value	17
5.	Trends in SPION magnetization	18
6.	Predicting non-linearities in SPION magnetic properties	21
7.	Geometric considerations for the model of SPION cluster magnetic properties	27
8.	Optimization of the important magnetic parameters for SPION cluster-proton interactions based on SPION size	32

LIST OF ABBREVIATIONS

B – magnetic field

BCRP – Breast Cancer Research Program

CDMRP – Congressionally Directed Medical Research Programs

χ – magnetic susceptibility

d – SPION inert shell thickness

EPR – enhanced permeability and retention

H – auxiliary magnetic fields

hcp – hexagonal close packing

k_b – Boltzmann's constant

M - magnetization

m – particle mass

m_0 – magnetic moment

MR – magnetic resonance

MRI – magnetic resonance imaging

M_{sat} – saturation magnetization

M_{spont} – spontaneous magnetization

M_{s0} – bulk saturation magnetization

r – particle radius

SPION – superparamagnetic iron oxide nanoparticle

T – temperature

T_c – Curie temperature

T2 – spin-spin relaxation time

T2* - corrected spin-spin relaxation time

USDoD – United States Department of Defense

μ - magnetic permeability

μ_0 – permeability of free space

V - particle volume

CHAPTER I

INTRODUCTION

In the rapidly expanding field of nanotechnology, few materials are under such strenuous and exhaustive investigation as nanoparticles. There are many types of nanoparticles under investigation for clinical and laboratory use and are generally categorized by their composition: silica, lipid, polymer, carbon, metal, and others. One of the largest categories of particles, metal nanoparticles, exhibit a wide range of functional properties ranging from useful chemical or biological activity, to unusual physical properties such as superparamagnetism. Superparamagnetism is a magnetic phenomenon observed in small metal and metal oxide particles that are small enough to have a single ordered magnetic domain. This creates a stronger magnetization in an applied field than multi-domain materials of the same size. In this work, the magnetic properties of superparamagnetic iron oxide nanoparticles (SPIONs) are investigated to create a mathematical model of SPION magnetic behavior in an applied magnetic field using experimental and first principle relationships. The proposed model is structured to predict magnetic properties using only particle size as its primary input, decreasing the burden of multiple iterations of particle design, fabrication, characterization, and re-design. Fundamentally, this model is an engineering design tool, of potential use by developers of novel materials utilizing SPIONs.

First, the efficacy and usefulness of SPIONs is evidenced in this work by their multiple current and potential clinical and laboratory uses. The phenomenon of superparamagnetism, the magnetic characteristic which gives these particles their uniquely strong magnetic fields, will then be described and the use of this model as a predictive engineering tool will be justified.

Next, the model itself will be presented, initialized by a set of well constrained physical and geometric parameters. The implications of the model for the magnetic properties of SPIONs as well as the model's predictive power will be discussed. Finally, an example how the model might be used will be presented, utilizing a geometrically simplified two dimensional model of novel nanomaterials in order to illustrate how the model might help to simplify the design problems inherent in a complex, nanoscale system with multiple design parameters.

Laboratory and clinical uses of iron oxide nanoparticles

Some laboratory uses of small magnetic particles

The use of small iron oxide particles as a laboratory or diagnostic tool has been practiced for almost 50 years [1]. The past two decades have seen dramatic improvement in the techniques used to fabricate and characterize iron oxide particles and there are currently several fabrication techniques that allow for the highly controlled and repeatable creation of ultra-small particles [1-6]. Though these materials garner much attention for their broad current and potential clinical uses, laboratory applications for these particles have significant utility. Commercially available particles can be used for labeling and magnetic separation of cells grown *in vitro* [7]. For this technique, magnetic particles can be targeted to a specific cell type via a surface expressed biorecognition molecule. The particles then associate with the target cell type, which then can be magnetically separated from other cells or imaged using a laboratory based magnetic imaging system. Many other examples of SPION applications in cell labeling and/or separation exist [8]. SPIONs can also be used for molecular detection of biological compounds [9]. In a manner similar to cellular labeling, SPIONs can be targeted to a specific molecule, enabling imaging or separation from solution. This technique has clear uses in

multiple fields: from answering fundamental biological questions, to screening molecules for national defense purposes. SPIONs may be used as a screening tool for novel biological compounds intended for clinical use, or as a materials' component [10, 11]. Is possible to utilize SPIONs as a high throughput screening agent for a specific desired biological activity among a cohort of candidate biomolecules [10].

Each of these applications depends on the magnetic properties of SPIONs to achieve sensing or detection in a predictable fashion. Optimization of these properties for a specific purpose is often lacking. Understanding how unique nanoscale phenomena modulate the controllable material characteristics limits the design of current and future SPION-based materials. An accurate model that allows the developers of these laboratory tools to leverage the nanoscale magnetic properties in a precise and accurate way would be a valuable design tool and allow for the creation of more sophisticated nanomaterials.

Some clinical uses of SPIONs

One of the most well known applications for SPIONs is for medical imaging contrast enhancement. SPIONs are a strong T2 and T2* contrast agent, producing dark negative contrast when they are employed for magnetic resonance imaging (MRI) [12]. Currently, SPIONs have been approved by various regulatory agencies around the world, primarily for the enhancement of liver lesions in MRI [13-15]. There exists a handful of approved imaging agents such as Feridex® and Resovist® for liver imaging that consist of SPIONs bound together in a larger biocompatible matrix, often made from dextran [16]. SPION-based contrast agents are particularly useful in that their efficacy as MRI contrast agents improves at higher applied field strengths, contrary to clinically used gadolinium based contrast agents, which exhibit decreasing efficacy at higher field strengths.

Other organs, such as the spleen, and systems, such as the lymph system, have also been investigated for image enhancement using a SPION based contrast agent [3, 17]. These applications generally utilize increased blood flow and vascular permeability to specific locations as the passive delivery mechanism for the SPIONs *in vivo*. Furthermore, the detection of cancerous lesions relies on the passive enhanced permeability and retention effect of solid tumors that increases the vascular permeability in these tissues as well as retains any nanoparticles that may be delivered [18]. This passive targeting technique is possible due to the irregular and leaky microvasculature present in these lesions.

In addition to differentiated image contrast enhancement of large, tissue scale pathologies, SPIONs are also potential contrast agents for *in vivo* cellular and molecular imaging [19, 20]. The biophysical properties of *in vivo* imaging are the same as *in vitro* imaging and detection. The SPIONs are targeted to a particular cell type or specific molecule and MRI is performed using T2 or T2* weighted scan [12, 19]. Using cellular imaging, it is possible to detect small amounts of a specific compound or a small mass of particular cells due to the micro-molar detection limit of SPIONs. Some scan sequences are capable of detecting single cells labeled with picograms of SPIONs at 100 x 100 x 200 um resolution [19]. This leverages the high spatial resolution of MRI with the enhanced sensitivity imparted by the nanomaterials [12]. Molecular and cellular imaging techniques using SPIONs as contrast agents allows for the imaging of pathologies that have never been imaged with MRI [21]. Newer techniques such as magnetic particle imaging, a modality that can image concentration gradients of SPIONs *in vivo*, enable increased spatial resolution [8, 22].

SPIONS have other, non-imaging clinical applications as well. A strong externally applied magnetic field, for example, can direct the movement of drug bearing ferrofluids to specific *in vivo* locations [23, 24]. The applied external field slows or stops the drug bearing

particles at the desired site, allowing for an increased dose to that region, lowering the overall required dose and side effects [25]. Understanding and controlling the magnetic force interactions between the particles and the applied field is a critical consideration for efficacious drug delivery [26]. Newer drug delivery techniques utilize implanted metal constructs such as vascular stents as targets for drug carrying SPIONs, which are attracted to the constructs when magnetized [27]. Other therapeutic applications include magnetic particle hyperthermia, which seeks to utilize the heat produced by SPIONs during magnetic energy deposition as a therapeutic tool to cause local cell heating and/or death [28]. Accurate and precise modeling of the magnetic properties of SPIONs is vitally important for efficacious material design of clinically useful SPION-based biomaterials.

Activatable MRI contrast agents

SPIONs used clinically as MRI adjuncts produce passive image contrast. The mechanism is passive in exhibiting the same physical, magnetic properties regardless of location or biological environment. Recently, novel SPION-based nanomaterials have come under investigation as activatable detection contrast agents. These activatable contrast agents can be nanoscale clusters of individual SPIONs, using a biomolecule sensitive to some predetermined biological event as a linking moiety [10, 11]. The cluster then becomes a switch which activates under the influence of a specific stimulus, creating a modulated MR signal. Studies have shown that the relaxation difference between the clustered aggregates and dispersed particles is significant enough to be detected by MRI as different amounts of image contrast [12, 29]. Active contrast agents represent a significant increase in complexity from traditional passive nanomaterials. As the amount of important, controllable parameters increases in the system,

the ability to predict the systemic effects of changes in these parameters using a model becomes more important.

An engineering model as a tool for material design

Modeling of natural phenomena has always been an important component of scientific discovery. A well designed model is even more important when it is used to aid the design and engineering of novel technologies. An engineering model becomes even more useful when the system or component which it models is itself difficult to directly interrogate or control due to its scale or complexity. Some techniques of nanomaterials development rely on the discovery of efficacious materials and leverage high throughput screening of a large number of candidate materials that may differ from one another in small ways. While high throughput discovery methods are appropriate for some aspects of nanomaterials development, a strong design developed before the first materials are fabricated can help to save both time and other resources. SPIONs have a wide range of controllable properties capable of utilization in varied biological systems. Creating the most efficacious SPIONs for a particular application is a complex problem, made even more difficult by the small scale of the materials which can make them difficult to characterize and implement. It is possible to simply stumble upon the ideal particle size, configuration, and magnetic properties for a given application using a high throughput screening technique, but a precise and accurate mathematical model of these physical phenomena would be a useful engineering tool to drive the design of these materials, rather than pure discovery. Such a model would lessen the burden of multiple material fabrication and characterization steps greatly facilitating the creation of SPION based nanomaterials ideally suited for a very specific purpose.

CHAPTER II

A MATHEMATICAL MODEL OF THE MAGNETIC PROPERTIES OF SUPERPARAMAGNETIC IRON OXIDE NANOPARTICLES

This work uses first principles of MR signal origins, superparamagnetism, and other magnetic phenomenon to develop a model of the magnetic behavior of superparamagnetic iron oxide nanoparticles and make predictions about MR signal modulation of these nanomaterials. One of the leading uses of SPIONs in magnetic resonance imaging is as a T2 or T2* contrast agent [19, 29]. T2 is the transverse relaxation that is created by decoherence in processional spin frequencies of protons following discontinuation of a strong magnetic pulse which initially aligns the direction and processional frequency of the proton spins. This decoherence is caused by fluctuations in the local magnetic field which are themselves created by the nuclear spins of nearby protons. T2* takes into account spin dephasing due to inhomogeneities in the applied magnetic field, and those caused locally by nearby magnetically active agents; therefore, SPIONs can be used as T2* contrast agents. Stronger and greater local magnetic field inhomogeneities induce faster the spin dephasing, creating stronger negative contrast in a traditional T2* weighted image [30].

Assumptions and initializing parameters

To begin the modeling effort, we started with a set of assumptions about the nanoparticle fabrication and about the biological environment in which the nanoparticles would exist during local magnetic field modulation. We assume that the particle fabrication method is thermal decomposition of iron pentacarbonyl, $Fe(CO)_5$, followed by oxidation of the resultant

magnetite to maghemite, γ-Fe_2O_3. We made this assumption based on our expertise in utilizing this fabrication method to produce SPIONs. This fabrication procedure produces spherical particles that are almost entirely composed of maghemite, as opposed to magnetite particles, which is another possibility for SPION composition [4]. This model may be applied for magnetite SPIONs through appropriate modifications in physical property data, principally the bulk saturation magnetization, M_{s0}, and the material density. The M_{s0} for maghemite is approximately 76 kA/m/g, whereas the value for magnetite is approximately 92 kA/m/g [31]. A larger magnetization will produce a stronger magnetic field, creating greater contrast. Magnetite is approximately 5.7% denser than maghemite. We further assume that the SPIONs will be acting at normal body temperature, 310 K, though this model is also applicable for temperature ranges of 150-340 K for maghemite and 150-430 K for magnetite [32, 33].

It is important to identify the physical characteristics of the particles including those that are controllable during fabrication. The bulk saturation magnetizations of the SPIONs are controlled by the iron oxide composition of the particle. Furthermore, the physical dimensions of the SPIONs are under very precise control; average size can be controlled within 1 nm increments by manipulating the ratio of reagents during the fabrication. The packing density of the SPIONs in dispersible clusters can be controlled by altering the composition and the size of the particle surface coat and linking moiety. An upper limit of 74% packing density for a cluster is imposed by the Kepler conjecture, a theorem establishing maximal packing of spheres. Cluster sizes of 50 nm in diameter were used for the modeling effort shown in CHAPTER IV [34]. This cluster size is in the range of clinically approved SPION-based nanomaterials and can be reproductively fabricated in our laboratory. Very small clusters are expected to behave much like individual particles and larger clusters (micron sizes) are less relevant for biological applications and may be produced by unwanted flocculation of particles or smaller clusters. A

simplistic cluster configuration would utilize SPION cores with a biocompatible coating and a cross-linking moiety on the surface to form the clusters as seen in **Figure 1.**

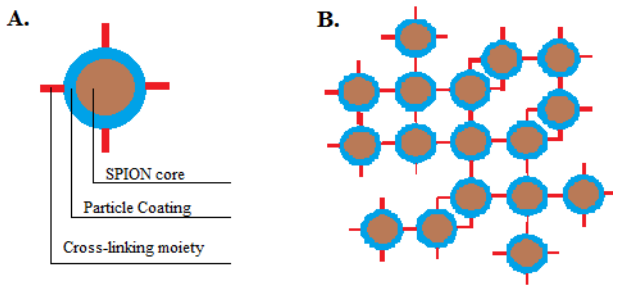

Figure 1: (A) A 2D representation of a single SPION coated for biocompatibility and containing a cross-linking moiety. (B) Diagram of a SPION cluster with cross-linked particles.

System temperature is a controllable parameter and is assumed to be 310 K. The size range of individual SPIONs chosen for interrogation within the model is based on the known superparamagnetic size range of iron oxide nanoparticles. A size range of 4 – 20 nm diameter particles was chosen because these values fall well within the superparamagnetic size range [35, 36]. Finally, the magnetic field applied to the SPIONs, which magnetize the particles to produce their own individual magnetic fields, is a controllable parameter. The magnetic field applied to the particles is assumed to be uniform, a valid assumption for MRI due to the fact that the magnetic field inside the bore of the MRI machine is approximately uniform. An applied field range of 0.001 – 3 Tesla was investigated. This range of field strengths was chosen so that the model might be applicable to both laboratory diagnostic and sensing techniques, as well as clinical MR imaging field strengths. **Table 1** summarizes the assumptions made for the model of individual SPION magnetic properties and speaks to the reasoning behind each assumption:

Table 1: Initializing assumptions for the model of SPION magnetization		
Parameter	Assumption/Value	Reason
particle geometry	spherical	Many fabrication methods produce spherical particles
particle size	4 - 20 nm	A range of values within the superparamagnetic range
particle composition	maghemite	A known superparamagnetic material; model is valid for others
temperature	310 K	Body temperature
applied magnetic field	invariant	Initial magnetizing pulse is invariant within the bore of an MRI
applied field strength	0.001 - 3 T	A range including field strengths including magnets used in laboratory techniques and clinical MRI

Determining the magnetization of an individual particle

The formulation of the model begins by estimating the saturation magnetization, M_{sat}, of an individual particle of a specific size. M_{sat} can be calculated for SPION based on the saturation magnetization of the bulk material (M_{s0}) composing the particle, in this case maghemite. A. Millan, *et al.* describe an experimental relationship which has M_{sat} as a function of M_{s0} and particle size [31]. This relationship, shown as equation 1, models a SPION as a core-shell particle with the magnetic properties of the particle coming from the core of the particle and a thin outer shell of magnetically inert material.

$$M_{sat} = mM_{s0}\left(\frac{r-d}{r}\right)^3, \quad (1)$$

where m is the mass of the individual particle, M_{s0} is the bulk saturation magnetization in A/m/g, r is the particle radius, and d is shell thickness, shown to be 1 nm for all superparamagnetic particle sizes [31]. Because d is invariably set to 1 nm, this model is only applicable for particle diameters larger than 2 nm. This experimental relationship gives the saturation magnetization of an individual particle in the SI units of A/m. It represents the maximum magnetization that a particle can undergo. Using M_{sat} it is possible to find the spontaneous magnetization, M_{spont}, which is an ordered magnetization in a particle that is present without any applied field.

$$M_{spont} = M_{sat}\left(1 - 0.3\left(\frac{T}{T_c}\right)^{1.2}\right), \quad (2)$$

where T is the temperature of the SPION and T_c is the Curie temperature of the bulk material. T_c is a transition temperature for magnetic materials. At temperatures above T_c, the material does not form ordered magnetic domains, and has no spontaneous magnetization. This relationship, discovered by G. I. Barinov, *et al.,* is valid for maghemite up to a temperature of $0.5T_c$ [32]. T_c for maghemite is 685 K, establishing a maximum valid temperature for this model of approximately 340 K.

Another key parameter of this model is the magnetic susceptibility of an individual particle. This dimensionless quantity is a fundamental material property that describes how a material will become magnetized in a magnetic field. The susceptibility, χ, of a nanoparticle is dependent on its volume, V, and temperature, T, as well as the M_{spont} of the particle as shown in equation 3 [33].

$$\chi = {M_{spont}}^2\left(\frac{\mu_0 V}{3k_b T}\right), \quad (3)$$

where μ_0 is the permeability of free space in SI units ($4\pi \times 10^{-7}$ N/A^2) and k_b is Boltzmann's constant (1.38065×10^{-23} J/K). The full description of a particle's magnetic susceptibility for all cases is quite complex and there are imaginary portions of the susceptibility that arise at temperatures lower than 150 K as well complex non-linear behavior for a particle in a dynamic field [33]. The system considered here justifies the simplifying assumptions that the particle is in an equilibrated magnetic field and that the temperature of the particle is higher than 150 K. These assumptions allow us to simplify the calculations for magnetic susceptibility into a single equation, equation 3 as shown above.

Finally, using the quantities found from the equations above, it is possible to estimate the magnetization of a single SPION in an applied magnetic field having knowledge only of the

particle size, temperature, and a few well known material properties. In order to simplify calculations, we have called the direction of the applied field the $\hat{z}$ direction. This means that the magnetization of a particle in this field will be solely in this direction as well. Another assumption is that the particles are spherical. The fabrication method of these particles, which proceeds by uniform growth of the particle around a nucleation point, as well as TEM images of the particles suggest this to be a valid assumption. The magnetization of a SPION has two components. The first component is best modeled by a Langevin type equation, which is a type of differential equation used to describe a stochastic process. This component takes into account the randomizing effect that temperature fluctuations might have on the magnetization of the particle. The second component is a linear relationship that takes into account the portion of the magnetization which is generated by paramagnetic behavior [37]. Normal paramagnetic materials (as opposed to superparamagnetic materials) as well as diamagnetic materials are liner media in that their magnetization increases linearly with the applied field. Traditionally, modeling work done in this field is described in terms of the cgs unit system and is done using the auxiliary magnetic field, $\vec{\mathrm{H}}$. In this manner, the magnetization of a nanoparticle, M, may be described as in equation 4:

$$M = M_{sat}\left(\coth\left(\frac{m_0 H}{k_b T}\right) - \frac{k_b T}{m_0 H}\right) + \chi H. \tag{4}$$

In this equation, H is the magnitude of the auxiliary field applied to the particles with SI units of A/m; the same units as M and M_{sat}. m_0 is the magnetic moment of the magnetic nanoparticle and can be found by solving equation 5 for m_0:

$$M_{sat} = \frac{n m_0}{V}. \tag{5}$$

The saturation magnetization also represents the magnetic moment per volume of a material at zero applied field multiplied by the number of magnetic moments, n. These particles are superparamagnetic and so have a single magnetic moment by definition (n=1). Therefore, m_0

may be found by multiplying the saturation magnetization by the particle volume and has SI units of Am^2.

When applying equation 4 to analyzing the magnetization of SPIONs in a uniform field, several issues arise. The first issue is that the auxiliary field, $\vec{H}$, is not the same as the magnetic field, $\vec{B}$. $\vec{B}$ is a fundamental property of a material that takes into account the total magnetic field attributable to the total current in the material, both bound current and free current. Bound current is a quantity that is inherent to the material; it cannot be turned on or off. Free current, the current that produces the auxiliary field, is the current which is under outside control and is therefore convenient to use in a laboratory setting when discussing the field of tunable electromagnets [38]. The field of an MR imaging instrument is produced by the total current in the magnet and is described in units of a $\vec{B}$ field, Teslas (T), and it is important to note that $\vec{H}$ is not the magnetic field. Furthermore, there is an issue of unit agreement in equation 4. The argument of the hyperbolic function, coth, should be a dimensionless quantity. The quantity inside the parentheses of the Langevin component should also be a dimensionless quantity that modulates the value of the saturation magnetization. As the equation is stated above, the SI units of the variables do not create dimensionless quantities in these cases. In order to rectify these and other issues stated previously, we have developed a modified form of equation 4:

$$M = M_{sat}\left(\coth\left(\frac{m_0 B}{k_b T}\right) - \frac{k_b T}{m_0 B}\right) + \frac{\chi}{\mu} B. \quad (6)$$

In this equation, the magnitude of the magnetic field, B, has replaced the magnitude of the auxiliary field, H. This allows for a realistic description of the magnetic phenomena of the SPIONs in an MRI's magnetic field, and solves the unit agreement issue described above. Also, a new term, μ, has been added to the equation in the linear term. μ is the magnetic permeability of an individual particle and can be found by using equation 7.

$$\mu \equiv \mu_0(1 + \chi) \tag{7}$$

The quantity $\frac{\chi}{\mu} B$ is analogous to χH for linear magnetic behavior [38].

By using equation 6, we can estimate the magnetization of a SPION in a magnetic field, keeping in mind that the direction of the vector quantity, $\overrightarrow{M}$, is in the same direction as the applied field, which we have arbitrarily called the $\hat{z}$ direction. The trends in particle magnetization are important tools that can be used to predict optimum particle size or applied field strength, based on the desired application.

Graphing the magnetic field of a SPION

Using the magnetization of a SPION determined as described above, is possible to determine the magnetic field produced by a single SPION in an applied field. By definition, SPIONs have a single magnetic domain, causing them to behave like a single magnetic dipole. This means that the equation for the magnetic field of a SPION is simply the equation for the magnetic field from a dipole:

$$\vec{B} = \frac{\mu_0 m_d}{4\pi r^3}\left(2\cos\theta \hat{r} + \sin\theta\, \hat{\theta}\right), \tag{8}$$

where r is the radial distance from the particle and θ is the angle away from the magnetization vector. In this case, m_d is the magnetic dipole moment, which is different from m_0 in equations 4 and 5 and can be found by using equation 9 and solving for m_d.

$$M = \frac{n m_d}{V}, \text{ n = 1} \tag{9}$$

By assuming a spherical particle shape and by invoking spherical symmetry it can be assumed that the magnetic field is invariant in the $\hat{\phi}$ direction of the spherical coordinate system. This assumption allows us to easily state equation 8 in terms of a Cartesian coordinate system:

$$\vec{B} = \frac{\mu_0 m_d}{4\pi r^3}(3\cos\theta \sin\theta\, \hat{y} + (2 - 3\sin^2\theta)\hat{z}) \quad (10)$$

Plotting the results of equation 10 creates a vector plot of the magnetic field around a single particle based on the particle size, magnetization (which is a function of particle size and applied field), distance from the particle, and the angle going away from the magnetization vector. **Figure 2** shows the vector magnetic field from a 20 nm SPION in a 1 T applied field. This is one example of how the model may be used for a specific particle size and applied field. Similar plots can be created using this model simply by changing initial assumptions of particle size and applied magnetic field.

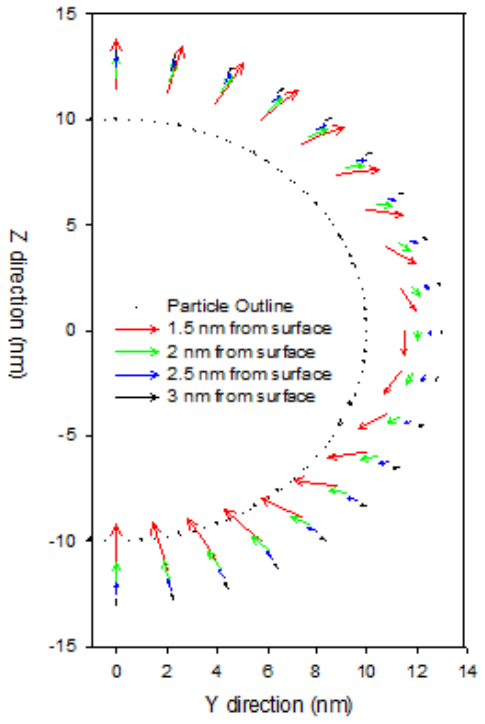

Figure 2: The vector magnetic field from a 20 nm SPION in a 1 T applied field.

The figure demonstrates that the model is able to faithfully reproduce the shape of the dipole magnetic field as well as the characteristic drop in the magnitude of the magnetic field as distance increases proportional to $\frac{1}{r^3}$. Furthermore, it is important to note that the magnitude of the magnetic field changes relatively little as θ changes for a given radial distance. In fact, the maximum magnitude of the magnetic field occurs along the vector of magnetization while the minimum that occurs along the vector perpendicular to the magnetization is only ½ of the maximum (**Figure 3**). It should be noted that the magnetic field from a single particle is very small. The bulk effect of SPIONs seen as MRI contrast or some other magnetic detection/separation device is due to millions, if not billions, of SPIONs acting together. The small field produced from a single SPION implies that the field from that particle only acts in a very local fashion.

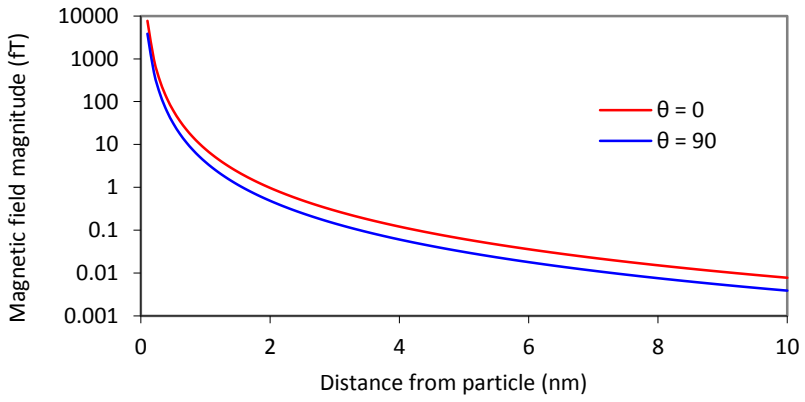

Figure 3: The magnitude of the magnetic field from a 20 nm SPION along a single radial line in a 1 T applied field. Two lines are shown: the first is 0° off from the magnetization vector (red), the second is 90° off from the magnetization vector (blue). These two lines represent the maximum and minimum values of the magnetization at a given radial distance.

CHAPTER III

RESULTS AND IMPLICATIONS OF THE MODEL

Magnetization trends

Once the trends in magnetization and magnetic fields produced by SPIONs are understood, it is possible to use the model to direct the design of nanoparticles ideally suited to a particular need. One key fact is made evident in the first stages of the model: the magnetic properties of SPIONs cannot be modeled accurately using the bulk characteristics of the materials. Due to unique, nanoscale phenomenon, the material properties of maghemite in nanoparticle form differ from its properties as a bulk material. Equation one exemplifies this by showing that the saturation magnetization of a SPION differs from the bulk saturation magnetization of the material by a geometric correction factor that modifies the bulk value to determine the nanoscale value. **Figure 4** shows how the saturation magnetization of a SPION differs from the bulk value of 76 kA/m/g as particle size decreases.

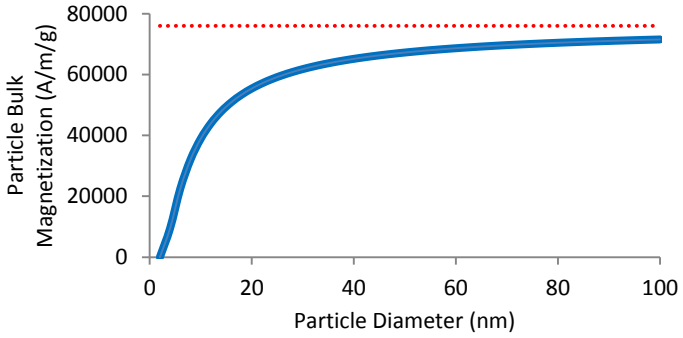

Figure 4: The saturation magnetization of a SPION (solid line) differs from the bulk material saturation magnetization (dotted line).

The other model equations confirm that other components of the particle magnetization are functions of the saturation magnetization, causing these components to also

be controlled by nanoscale phenomenon. Furthermore, these components are themselves functions of particle geometry, either particle radius or volume, compounding the nanoscale effect on these properties. For example, the magnetic susceptibility is a function of particle volume as well as the spontaneous magnetization, which is itself a function of the saturation magnetization. Due to the multiple instances of nanoscale effects which appear in the model, the ultimate magnetization of a SPION in an applied magnetic field cannot be predicted by extrapolating the bulk properties to a sample of SPIONs. The final model equation for particle magnetization, equation 6, predicts important trends in SPION magnetization.

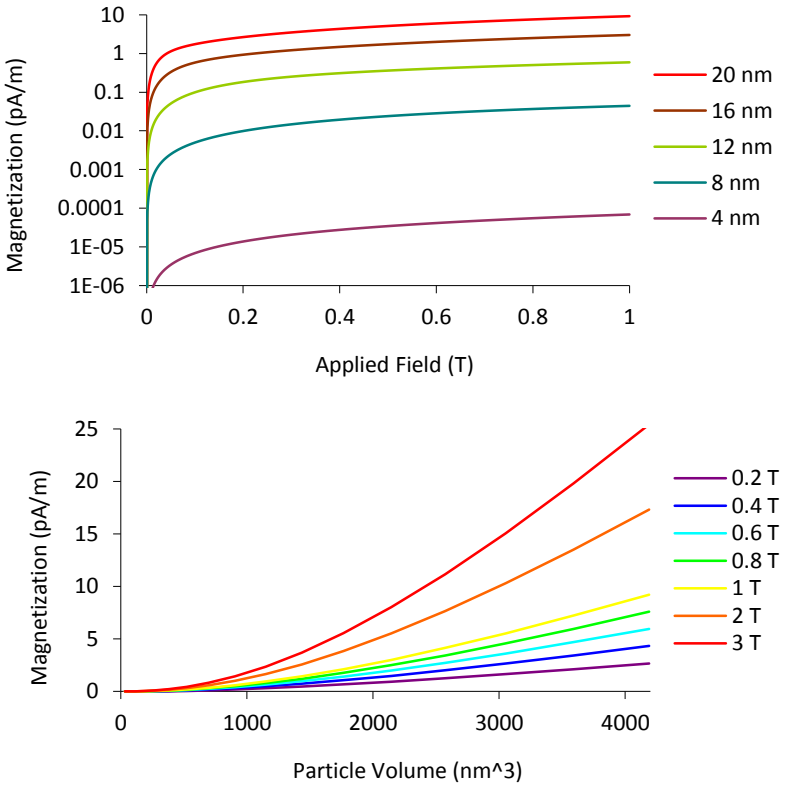

Figure 5: These graphs show the trends in SPION magnetization as a function of applied field and particle volume. For a given applied field, the magnetization of a particle increases with particle size. Similarly, for a given particle size, the magnetization increases as the applied field increases.

One conclusion is that particle magnetization increases as particle size and applied field increase. As particle size decreases, the difference between magnetization at a given field for the particle as compared to larger particles increases. In other words, the magnetization decreases, but the rate of change increases. The magnetization at 1T between a 4 nm and an 8 nm particle differs by several orders of magnitude, while the magnetization between 8 nm and 12 nm particles differs by approximately one order of magnitude. It is important to note though, that the absolute differences in magnetization are still greater between larger particles. The fact that the relative difference in magnetization is largest for smaller particles but the absolute difference is largest for larger particles is a trend that could potentially be used by developers of novel nanomaterials attempting to produce samples of SPIONs with differential characteristics. **Figure 5** also documents that the magnetization of a SPION is much more sensitive to changes in particle size than changes in the applied field. This allows us to conclude that inhomogeneities in an applied magnetic field will not affect the performance of SPION based contrast agents as much as the size of the particles, which is under very precise control during the fabrication process as shown by dynamic light scattering measurements and electron microscopy. For example, a 6 nm particle in a 1 T applied field is estimated to have a magnetization of 0.004345 pA/m. If the applied field is tripled the magnetization increases to 0.01199 pA/m, an increase of almost a half order of magnitude. However, if the size is tripled the magnetization increases to 5.536 pA/m, an increase of over three orders of magnitude. This is useful because it means that the magnetic properties of the SPIONs are principally controlled by the fabrication process, and are only weakly susceptible to magnetic field inhomogeneities that may be present in the applied magnetic field. On the other hand, this also can be viewed as a disadvantage because there can be little fine tuning of the magnetic response of the particles after fabrication by modulation of the applied field.

Investigations into the magnetic properties of SPIONs have only recently been able to measure or calculate the magnetic moment of an individual SPION by using a superconducting quantum interference device-based magnetometer [39]. This study was done using hematite nanoparticles (α-Fe_2O_3), but it is possible to use known relationships between hematite and maghemite nanoparticles to extrapolate the measured hematite nanoparticle magnetic moment to maghemite SPIONs. The magnetic moment of a 7 nm diameter hematite particle at 300 K in a 50 mT applied field was found to be approximately 300 Bohr magnetons or $2.7*10^{-21}$ Am^2 [39, 40]. At 300 K the magnetization of maghemite SPIONs is approximately twice the magnetization of hematite particles of the same size [5], making the magnetic moment of the maghemite particles $5.56*10^{-21}$ Am^2. Our model predicts the magnetic moment of a 7 nm maghemite particle to be $4.97*10^{-21}$ Am^2. The 11% difference in the values can be explained by different assumptions made by the experimental study comparing the two types of iron oxide and our model. Our model assumes perfectly spherical particles while the study comparing hematite and maghemite particles utilized slightly rod shaped particles. The shape anisotropy effects results in a slightly different relationship between the two particle types as compared to the relationship between perfectly spherical particles [5].

Predicting linearity of magnetic behavior

This model enables assessment of the linearity of SPION magnetic properties as a function of particle size or applied field. The non-linear Langevin component of SPION magnetization can be assed relative to the linear contribution using this model. The ratio of these two components is an indicator of the linearity of the SPION's magnetic properties in an applied field. A particle for which the Langevin component is largely dominant can be said to be very non-linear, whereas the opposite would be true for a particle in which the Langevin

component is only a small percentage of the total magnetization. A high or low degree of linearity for a particle is neither good nor bad; the ability to predict the linearity of particle magnetic behavior is another design tool that can be used for material design and fabrication. A good design will exploit these material properties to increase the efficacy of the SPIONs for a particular application.

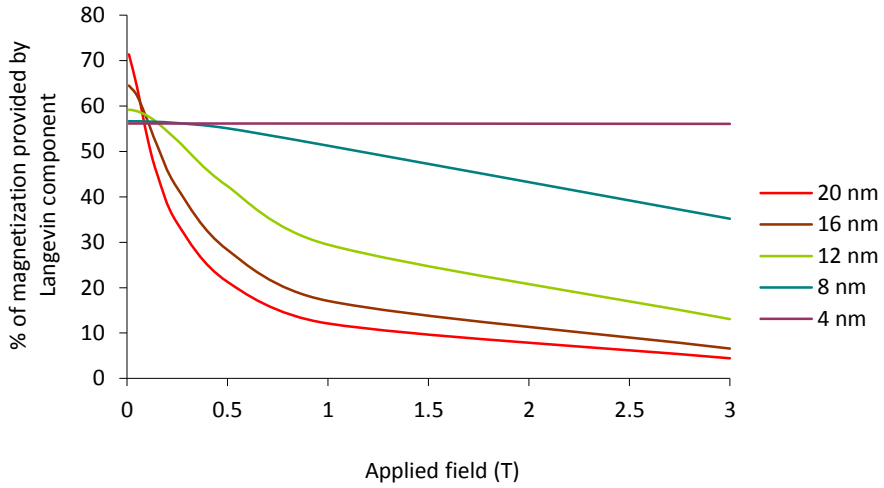

Figure 6: The Langevin component of the magnetization for different particles expressed as a percentage of the total magnetization. The % of the magnetization provided by the Langevin component is an indicator of non-linear behavior of a SPION in a magnetic field.

The degree of non-linearity is similar among all superparamagnetic particle sizes for applied fields round 0.3 T (**Figure 6**). Larger particles have a greter degree of non-linearity for smaller field strengths (such as those that might be used for molecular sensing or other laboratory diagnostics/tools) but very rapidly become dominated by the linear portion of the magnetization at larger field strengths. The non-linearity in smaller particles changes less across the field strengths investigated. Note that non-linearity is almost invariant with regards to applied field strength for the 4 nm particle.

The ability to predict linearity of particle magnetic properties is useful because there may exist applications for which linear materials are preferred to non-linear materials and vice versa. Linear materials exhibit a directly proportional relationship between the applied field and the magnetization of the particles. Non-linear materials can exhibit large rates of change, allowing for large changes in material properties with relatively small changes in the factors that control these properties. For example, small SPIONs have largely non-linear magnetizations at MRI field strengths. This model shows that the degree of non-linearity can be tuned during particle fabrication and influenced later by applied field strength. The model evokes the idea of optimum physical property and operating regimes that provide the characteristics specified in a particular design.

CHAPTER IV

USING THE MODEL TO DESIGN NOVEL NANOMATERIALS: A 2D EXTRAPOLATION OF A CLUSTERED PARTICLE SYSTEM

Preliminary steps for model utilization: a priori knowledge of desired SPION activity

Nanomaterial design must be informed by the target biological system properties. The optimal magnetic characteristics must also be defined in the case of SPION material design as a detection or therapeutic adjunct. Living system characteristics have a profound effect on temporal and spatial SPION distribution. From a design perspective there is often a preferred tissue location for action of SPIONs. The delivery of SPIONs to the target tissue can be influenced by the route of administration. For intravenous delivery, preferential tissue interaction can be mediated by biochemical ligand-receptor interactions that leverage unique cell surface composition of particular tissues. Physical targeting can be achieved by utilizing differential vascular permeability present in some tissues. For example, tumors often possess leaky, disorganized vasculature caused by rapid, irregular angiogenesis. This leaky vasculature facilitates delivery of appropriately sized SPIONs to the tissue via the enhanced permeability and retention (EPR) effect [41]. Tumor blood vessels are formed with large fenestrations in the vascular wall. By determining the average size of the vessel gaps, the optimal particle size for escape from tumor vasculature can be estimated and used to guide material design. The result can be an increase in tumor concentration of SPIONs that produce a dense spatial distribution of nanomaterials in the tumor.

Antithetically, the biological and material properties that optimize SPION delivery to tumor tissue are not optimal for delivery to tissues such as the brain. From an intravenous infusion, SPIONs must pass the blood-brain barrier, a major physical transport obstacle for even

nanoparticle delivery. Using tumor optimized SPIONs for brain targeting would most likely result in low concentrations and spatial distributions of the SPIONs at the target site. It would be necessary to alter particle size and other parameters in order to facilitate transport across the blood brain barrier. It is important to note that particle size will be largely dictated by biology and therefore has implications for the magnetic behavior of the final nanomaterials. In addition to knowledge of the target biological phenomenon, it is important to have some understanding of what type of magnetic phenomenon would be most efficacious for a given application. With this initial knowledge, it is then possible to use the model to design nanomaterials to fit the desired behavior.

Geometric considerations for 2D cluster modeling

A number of proposed magnetic materials utilize clustered SPIONs as active image contrast agents. These materials have multiple controllable geometric parameters which directly impact their magnetic properties in the clustered and dispersed orientations. Cluster size and shape, as well as SPION size and packing density, will affect the magnetic properties of the fabricated materials. Individual SPIONs possess magnetic characteristics that are dependent on size and applied field strength. The presence of other SPIONs in a cluster can affect the net field from other SPIONs in a constructive or destructive fashion, depending on proximity and orientation.

We have developed a simplified model of a 2D SPION cluster that reflect important physical characteristics of a 3D cluster and evaluates magnetic field estimates as in our model. In a 3D spherical system, the maximum packing density of spherical particles inside a cluster is constrained by the Kepler conjecture to be approximately 74% [34]. The SPIONs inside a maximally packed cluster can take either a face-centered close pack or a hexagonal close pack

[34]. For this model we have utilized a hexagonal close pack of SPIONs and have assumed the limiting case of maximum packing. A face centered close pack is also capable of producing a maximum packing density. A hexagonal close pack was chosen because this arrangement produces more spherical clusters than a face centered close pack which is more appropriate for use in living systems. Even with maximum packing, there is significant volume inside the cluster that is not occupied by SPIONs. This volume represents void space in which water and other molecules may enter and interact with the cluster. Internalized water molecules play a critical role in the MR signal modulating properties of SPION nanomaterials. While it is true that the magnitude of the magnetic fields from the particles decreases rapidly with distance, it is desirable that the maximum magnitude of the net magnetic field experienced by a hydrogen inside the cluster is similar to the maximum net field experienced a hydrogen surrounding the cluster. This would result in more uniform MR signal modulation for a given cluster and would ensure that the volume of water inside the cluster is affected in a fashion similar to the volume of water within the proximity of the cluster.

The maximum net magnetic field magnitude experienced by a hydrogen contributes significantly to the demodulation of the processional frequency of the proton spin [30]. The net field acting on a hydrogen is proportional to the field strength of the SPIONs interacting with it and is maximized for the closest approach of water to a SPION. In order to estimate this minimum distance, the spatial characteristics of a water molecule and the geometry of the water-SPION interactions must be considered. A water molecule may be modeled as a sphere having an average radius of 0.19 nm [42]. We assume that the spatial characteristics between a water molecule and a SPION will be controlled by oxygen-iron oxide interactions. This assumption is based on the significant volume fraction of oxygen in the water and the lack of hydrogen atoms bonding with the SPION particle. We assume no H-H bonding between the

SPIONs and water molecules due to the lack of hydrogen atoms in the SPION. We have assumed that the closest approach of a water molecule to a SPION is the distance of the Fe-O bond in the maghemite particle. This bond length is 0.2 nm, resulting in a water-SPION minimum distance of 0.39 nm [43]. This orientation yields the maximum magnetic field experienced by a hydrogen in a water molecule associated with a SPION.

The water molecule distance constraint also allows us to remove some particle sizes from consideration as candidates for optimum cluster components. Assuming hexagonal close packing (hcp) geometry enables characterization of the spatial distribution of the void space in the cluster. In an hcp packed cluster, any three SPIONs form an equilateral triangle with the particle centers serving as the vertices of the triangle. The contact points of the particles also form an equilateral triangle; the center of this triangle is the center of the void space between the SPIONs. Geometric principles enable identification of distances in an hcp cluster, including the distance from a SPION to the center of the void, the location where we have modeled the position of an internalized water molecule [44, 45]. **Figure 7** illustrates the geometry of the hcp particle cluster, geometrically simplified to a 2D system.

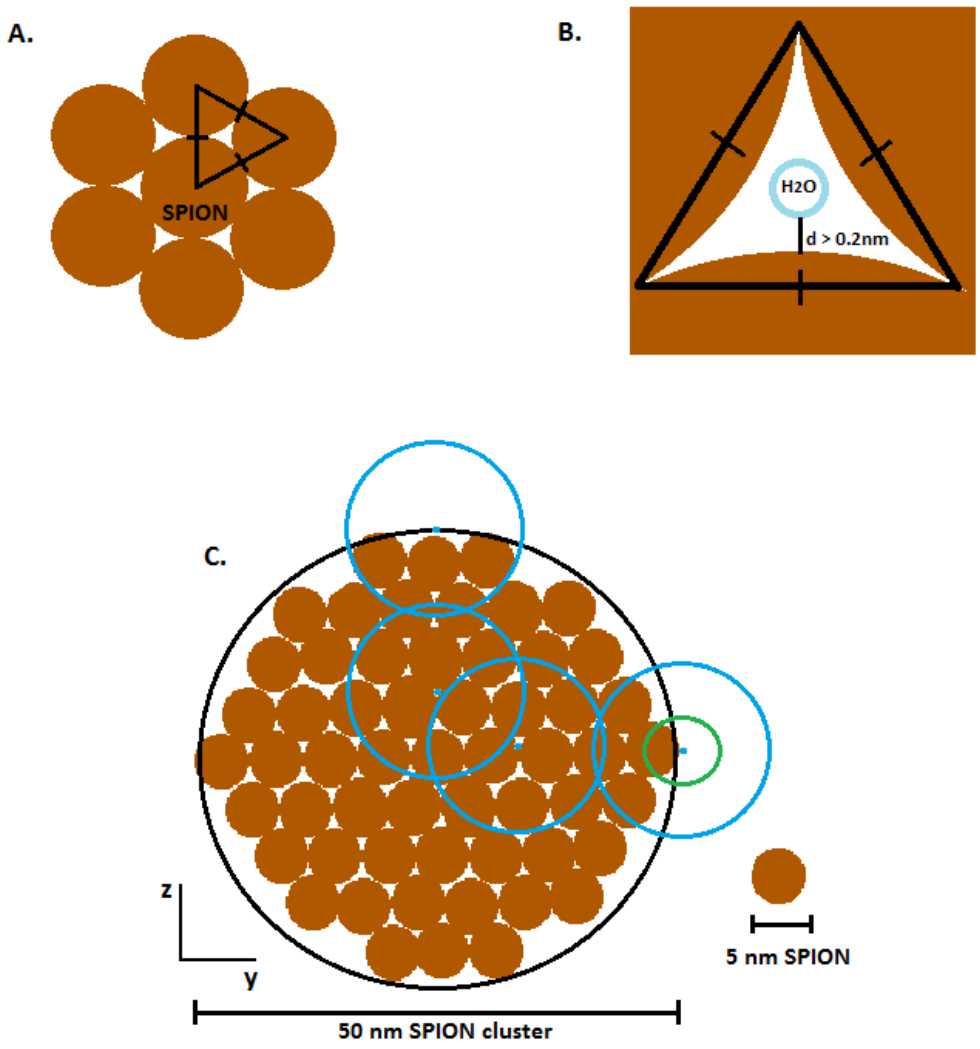

Figure 7: Geometric considerations for the model of SPION cluster magnetic properties. (A) Unit cell of an hcp scheme for particle arrangement inside a cluster. The centers of any three particles form an equilateral triangle. (B) Magnified view of the void space between three particles with a water molecule inside. The surfaces of the SPIONs form a hyperbolic equilateral triangle around the void allowing facile determination of the void's center. Due to geometric constraints caused by water-particle interactions, the minimum distance from a SPION to the void center is 0.39 nm. (C) Cartoon of the modeled particle cluster with internal and external water molecules shown at the positions used for modeling purposes. A radius of interaction (blue circle) was predicted for the water molecules which described the distance for which the magnetic field experienced from a single SPION was within 0.01% of the maximum magnitude. A second radius is shown for a distance representing 0.1% of the maximum field magnitude (green circle). A 50 nm cluster size was chosen to mimic the size of clinically used SPION clusters. The z direction is the direction of the magnetization imposed by the applied magnetic field.

Figure 7 also illustrates how water molecules are spatially arranged in this model. Four water molecule locations were examined: two inside the cluster in the void space and two outside the cluster at the minimum distance. Positions were either 0° or 90° relative to the

magnetization vector. We disregard magnetic field contributions less than 0.01% of the maximum magnitude. A sensitivity analysis of other limiting contributions would, perhaps, provide a different assumption; here we simply demonstrate the mathematical model capabilities. The magnetic field magnitude constraint provides a radius of interaction between each water molecule and local SPIONs. Using the minimum distance of 0.39 nm between a water molecule center and a SPION, it is possible to solve the system of equations for the magnitude of a SPION magnetic field to determine the distance at which the magnetic field reaches 0.01% of its maximum value. The magnetic field strength decreases proportional to $\frac{1}{r^3}$. To find the distance at which the field strength reaches 0.01% of its maximum value, occurring at 0.39 nm from a SPION surface, the minimum distance is multiplied by the cubed root of 10,000. This maximum distance is 8.6 nm and establishes a radius of interaction for the model independent of SPION diameter.

Clusters composed of larger individual SPIONs may yield circumstances in which a water molecule interacts with a single SPION within its radius of interaction. A cluster with smaller particles may have more SPIONs interacting with a particular water molecule, but the magnitude of each magnetic field will be smaller. For this case there are multiple magnetic fields acting to dephase the processional frequency of the proton spin. For this reason, the number of magnetic fields affecting a water molecule is an important design parameter. The complex interactions among SPION sizes and magnetic field geometries contribute to the difficulty in identifying optimal design characteristics *a priori*.

Estimation of ideal particle size

Based on our assumptions, the water molecule center must maintain a distance of at least 0.39 nm from a SPION surface. Thus, water molecules would not be able to enter into hcp

clusters composed of SPIONs smaller than 6 nm in diameter because the void spaces created in such a cluster would be too small. For the purposes of the clustered system which we are modeling, it is important to the functionality of the nanomaterials that water molecules be able to interact with SPIONs inside the cluster. This represents a significant volume for water molecules to occupy relative to the volume outside the particle constrained by a shell 8.6 nm distant from the SPION surface.

The symmetries inherent in spherical particles and in ideally spherical hcp clusters of particles allow us to simplify the 3D cluster into a 2D system as shown in **Figure 7c**. The spatial geometry of the cluster remains the same, and the volumetric considerations become simplified to area considerations. In 2D, the maximum packing density still occurs with an hcp formation, and the maximum packing density becomes 90.69% [46]. The area not occupied by the SPIONs is still substantially large as compared to the area bounded by a shell 8.6 nm from the particle surface, evidence that the water molecules in the void space make a substantial contribution to the proton-SPION interactions even in a simplified 2D system. Recalling **Figure 3,** the magnetic field strength outside a cluster decreases proportional to $\frac{1}{r^3}$. The same relationship does not occur inside the void space of the cluster because as a water molecule moves away from the void space center, its average location, it becomes more distant from one particle, but closer to others. This effect occurs due to the water-SPION proximity in the void and the consequent contribution of proton dephasing from multiple SPIONs. This shows the importance of inter-cluster protons in producing the magnetic phenomena desired from the nanomaterials. Using the mathematical model of particle magnetization, we can analyze the magnetic properties and water-SPION interactions of clustered SPIONs of different sizes in a 50 nm cluster in a 1 T applied field. This allows for the determination of the optimum size given our assumptions and other constraints. Several parameters contribute to optimum nanoparticle size:

- The maximum magnitude of the net magnetic field experienced by water molecules interacting with the cluster

The maximum net field strength will occur when a water molecule is closest to a SPION surface and is 0° relative to the magnetization vector. This maximum net field strength will be greatest for large particle sizes.

- Uniformity of maximum magnetic field strengths inside and outside the particle

The maximum field strength, occurring just outside the cluster, controls the SPION-proton interactions more than the weaker field inside the cluster. It is important for the cluster's magnetic uniformity that the maximum field strengths inside and outside the cluster are similar. The amount of water inside the cluster represents of significant area for the 2D cluster model, comprising 10-20% of the total water. Smaller particles have similar maximum field strengths inside and outside the cluster. As the void space becomes smaller, the average distance between a water molecule and a SPION surface becomes smaller. As the water molecule approaches the minimum distance from the internal SPIONs the maximum net field strength experienced by a given proton in the void approaches the overall maximum value.

- The number of SPIONs within a water molecule's radius of interaction

Not only the net magnetic field, but also the number of individual fields experienced by a proton act to dephase its processional frequency relative to other protons. This situation is analogous to the spinning proton being pulled strongly in one direction versus it being pulled moderately in many directions. The number of SPIONs able to affect a water molecule within its 8.6 nm radius of interaction also increases as particle size decreases.

In order determine ideal SPION size, the net magnetic fields experienced by water molecules at the four locations described previously and shown in **Figure 7c** were analyzed for 50 nm clusters assembled from particles sized 6-20 nm in 1 nm increments. Simulation results reveal the magnetic field experienced by water molecules located inside the cluster void spaces (average location in the center of the void space) is uniform regardless of position relative to the magnetization vector direction. This result differs from the individual SPION behavior in which the magnetic field is modulated by the orientation relative to the magnetization vector. The symmetry of an hcp arranged cluster equalizes the magnetic field magnitudes and directions experienced by water molecules irrespective of magnetization vector orientation. These characteristics maintain a net uniform magnetic field inside the cluster. The net magnetic field experienced by a proton outside the cluster and 90° relative to the magnetization vector is opposite in direction and ½ the magnitude of that experienced by a proton at the same distance 0° or 180° relative to the magnetization vector. This behavior is conserved regardless of the number of magnetic fields acting on the proton. This interaction, caused again by the geometrical symmetry of the cluster, is interesting in that it is the same behavior shown by an individual SPION, indicating that a nanoparticle cluster might be appropriately modeled as a single partical for larger scale interaction.

The global performance optimum is produced by the superposition of multiple individual contributions. The relationships among physical properties and cluster performance are nonlinear and, in some cases, inversely proportional. For example, the field experienced by a proton is maximal for the largest SPION, but this characteristic minimizes the number of SPIONs that influence a given hydrogen. **Figure 8** shows the result of this investigation plotted in a single figure:

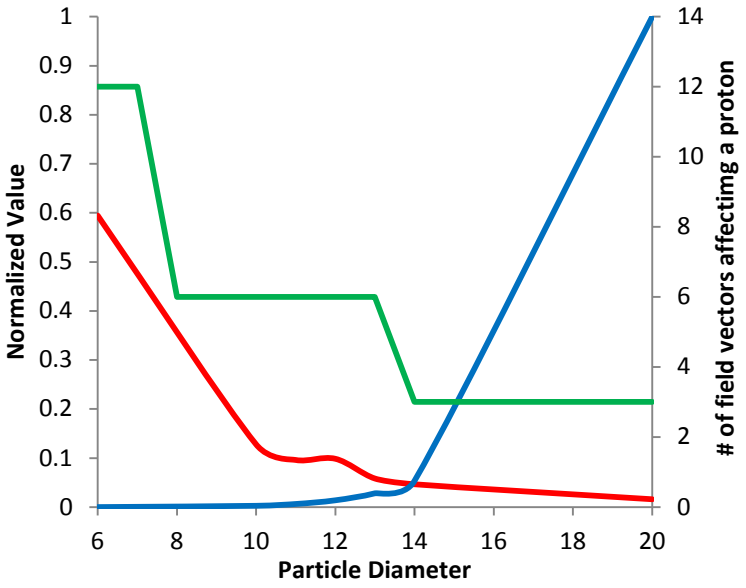

Figure 8: Optimization of the important magnetic parameters for SPION cluster-proton interactions based on SPION size. Two parameters are presented in a normalized fashion: the maximum magnetic field magnitude inside a cluster has been normalized to the absolute maximum magnitude for that cluster (red) and the absolute maximum field magnitude felt in each cluster of different size SPIONs has been normalized to the maximum field strength from a 20 nm SPION cluster (blue). A normalized value of 1 on the left x-axis is the ideal value for these parameters. The maximum number of magnetic fields acting on a proton for a given cluster is shown in green. The highest value is the most ideal for this parameter.

As the individual SPION diameter increases, the field experienced by an adjacent proton also increases; however, geometric constraints reduce the number of SPIONs influencing each proton. Furthermore, as SPION diameter decreases, the magnetic field inside the cluster approaches the maximum value experienced outside the cluster. This value is a measure magnetic property uniformity for an individual cluster. These competing values create a classic optimization problem. Using an optimization plot like **Figure 8**, it is possible to guide the design of SPION based nanomaterials to select a specific parameter to optimize to create the most efficacious materials for a particular purpose.

CHAPTER V

CONCLUSIONS AND FUTURE WORK

The goal of this work is to develop and demonstrate a novel model of superparamagnetic iron oxide nanoparticle magnetic properties based on physical first principles and experimental mathematical relationships. The developed model is able to predict the magnetic properties of any type of SPION at a given temperature and applied field strength based solely on the particle size. By predicting SPION magnetization and induced magnetic field, the model is a useful engineering tool for nanomaterials design. Using the model, it is possible to predict the magnetic behavior of even complex SPION based nanomaterials, facilitating materials design rather than pure discovery using costly high throughput methods. Using this model, we have investigated the magnetic properties of a clustered system of SPIONs to potentially be used as a magnetic detection device and image contrast agent. Within the model, we can predict ideal particle size for these particular nanomaterials by optimizing key magnetic parameters.

Future work with this model can be as varied as there are applications for magnetic nanoparticles. Specifically, the model will be used to aid in the design of active MRI contrast agents for the early detection of localized cancerous tumors and metastases. The 2D model presented here will be extrapolated to a 3D system and potential inhomogeneities in cluster geometry will be taken into account using the idealized, highly symmetric hcp structured cluster modeled here as a starting point.

BIBLIOGRAPHY

1. Gupta, A.K. and M. Gupta, *Synthesis and surface engineering of iron oxide nanoparticles for biomedical applications.* Biomaterials, 2005. **26**(18): p. 3995-4021.

2. Zhao, Y.M., et al., *Growth and characterization of iron oxide nanorods/nanobelts prepared by a simple iron-water reaction.* Small, 2006. **2**(3): p. 422-427.

3. Weissleder, R., et al., *Ultrasmall Superparamagnetic Iron-Oxide - an Intravenous Contrast Agent for Assessing Lymph-Nodes with Mr Imaging.* Radiology, 1990. **175**(2): p. 494-498.

4. Woo, K., et al., *Easy synthesis and magnetic properties of iron oxide nanoparticles.* Chemistry of Materials, 2004. **16**(14): p. 2814-2818.

5. Woo, K. and H.J. Lee, *Synthesis and magnetism of hematite and maghemite nanoparticles.* Journal of Magnetism and Magnetic Materials, 2004. **272**: p. E1155-E1156.

6. Muller, R., et al., *Precipitated iron oxide particles by cyclic growth.* Zeitschrift Fur Physikalische Chemie-International Journal of Research in Physical Chemistry & Chemical Physics, 2006. **220**(1): p. 51-57.

7. Arbab, A.S., et al., *Labeling of cells with ferumoxides-protamine sulfate complexes does not inhibit function or differentiation capacity of hematopoietic or mesenchymal stem cells.* Nmr in Biomedicine, 2005. **18**(8): p. 553-559.

8. Cantillon-Murphy, P., et al., *Measuring SPIO and Gd contrast agent magnetization using 3 T MRI.* Nmr in Biomedicine, 2009. **22**(8): p. 891-897.

9. Dave, S.R. and X.H. Gao, *Monodisperse magnetic nanoparticles for biodetection, imaging, and drug delivery: a versatile and evolving technology.* Wiley Interdisciplinary Reviews-Nanomedicine and Nanobiotechnology, 2009. **1**(6): p. 583-609.

10. Perez, J.M., et al., *DNA-based magnetic nanoparticle assembly acts as a magnetic relaxation nanoswitch allowing screening of DNA-cleaving agents.* Journal of the American Chemical Society, 2002. **124**(12): p. 2856-2857.

11. Josephson, L., J.M. Perez, and R. Weissleder, *Magnetic nanosensors for the detection of oligonucleotide sequences.* Angewandte Chemie-International Edition, 2001. **40**(17): p. 3204-+.

12. Roca, A.G., et al., *Effect of Nanoparticle and Aggregate Size on the Relaxometric Properties of MR Contrast Agents Based on High Quality Magnetite Nanoparticles.* Journal of Physical Chemistry B, 2009. **113**(19): p. 7033-7039.

13. Reimer, P., et al., *Receptor Imaging - Application to Mr Imaging of Liver-Cancer.* Radiology, 1990. **177**(3): p. 729-734.

14. Harisinghani, M.G., et al., *MRI contrast agents for evaluating focal hepatic lesions.* Clinical Radiology, 2001. **56**(9): p. 714-725.

15. Stark, D.D., et al., *Superparamagnetic Iron-Oxide - Clinical-Application as a Contrast Agent for Mr Imaging of the Liver.* Radiology, 1988. **168**(2): p. 297-301.

16. Santoro, L., et al., *Resovist Enhanced MR Imaging of the Liver: Does Quantitative Assessment Help in Focal Lesion Classification and Characterization?* Journal of Magnetic Resonance Imaging, 2009. **30**(5): p. 1012-1020.

17. Rummeny, E., et al., *Mr Imaging of Focal Lesions of Liver and Spleen - Application of Ferrite, a New Res-Specific Contrast Agent.* Radiologe, 1988. **28**(8): p. 380-386.

18. Decuzzi, P. and M. Ferrari, *Design maps for nanoparticles targeting the diseased microvasculature.* Biomaterials, 2008. **29**(3): p. 377-84.

19. Bulte, J.W.M. and D.L. Kraitchman, *Iron oxide MR contrast agents for molecular and cellular imaging.* Nmr in Biomedicine, 2004. **17**(7): p. 484-499.

20. Lanza, G.M., et al., *Molecular imaging and targeted drug delivery: A new paradigm in medicine.* Abstracts of Papers of the American Chemical Society, 2003. **226**: p. U473-U473.

21. Simon, G.H., et al., *Ultrasmall supraparamagnetic iron oxide-enhanced magnetic resonance imaging of antigen-induced arthritis - A comparative study between SHUSSSC, ferumoxtran-10, and ferumoxytol.* Investigative Radiology, 2006. **41**(1): p. 45-51.

22. Gleich, B. and R. Weizenecker, *Tomographic imaging using the nonlinear response of magnetic particles.* Nature, 2005. **435**(7046): p. 1214-1217.

23. Lubbe, A.S., et al., *Preclinical experiences with magnetic drug targeting: Tolerance and efficacy.* Cancer Research, 1996. **56**(20): p. 4694-4701.

24. Lubbe, A.S., et al., *Clinical experiences with magnetic drag targeting: A phase I study with 4'-epidoxorubicin in 14 patients with advanced solid tumors.* Cancer Research, 1996. **56**(20): p. 4686-4693.

25. Haverkort, J.W., S. Kenjeres, and C.R. Kleijn, *Computational Simulations of Magnetic Particle Capture in Arterial Flows.* Annals of Biomedical Engineering, 2009. **37**(12): p. 2436-2448.

26. Kuhn, S.J., D.E. Hallahan, and T.D. Giorgio, *Characterization of superparamagnetic nanoparticle interactions with extracellular matrix in an in vitro system.* Annals of Biomedical Engineering, 2006. **34**(1): p. 51-58.

27. Forbes, Z.G., et al., *Validation of high gradient magnetic field based drug delivery to magnetizable implants under flow.* Ieee Transactions on Biomedical Engineering, 2008. **55**(2): p. 643-649.

28. Hergt, R., et al., *Magnetic particle hyperthermia: nanoparticle magnetism and materials development for cancer therapy.* Journal of Physics-Condensed Matter, 2006. **18**(38): p. S2919-S2934.

29. Tanimoto, A., et al., *Relaxation effects of clustered particles.* Journal of Magnetic Resonance Imaging, 2001. **14**(1): p. 72-77.

30. Webb, A., ed. *Introduction to Biomedical Imaging*. IEEE Press Series in Biomedical Engineering, ed. M. Akay. 2003, John Wiley & Sons, Inc.: Hoboken, NJ.

31. Millan, A., et al., *Surface effects in maghemite nanoparticles.* Journal of Magnetism and Magnetic Materials, 2007. **312**(1): p. L5-L9.

32. Barinov, G.I. and S.S. Aplesnin, *Change in the critical exponent of magnetization in maghemite in the temperature range of the structural phase transition.* Physics of the Solid State, 2006. **48**(1): p. 84-87.

33. Jonsson, P., et al., *Nonlinear dynamic susceptibilities of interacting and noninteracting magnetic nanoparticles.* Journal of Magnetism and Magnetic Materials, 2000. **222**(1-2): p. 219-226.

34. Hales, T.C., *A proof of the Kepler conjecture.* Annals of Mathematics, 2005. **162**(3): p. 1065-1185.

35. Butler, R.F. and S.K. Banerjee, *Theoretical Single-Domain Grain-Size Range in Magnetite and Titanomagnetite.* Journal of Geophysical Research, 1975. **80**(29): p. 4049-4058.

36. Sjogren, C.E., et al., *Crystal size and properties of superparamagnetic iron oxide (SPIO) particles.* Magnetic Resonance Imaging, 1997. **15**(1): p. 55-67.

37. Gilbert, I., et al., *Magnetic properties of maghemite nanoparticles in a polyvinylpyridine matrix.* Polyhedron, 2003. **22**(14-17): p. 2457-2461.

38. Griffiths, D.J., *Introduction to electrodynamics*. 3rd ed. 1999, Upper Saddle River, N.J.: Prentice Hall. xv, 576 p.

39. Zelenakova, A., J. Kovac, and V. Zelenak, *Magnetic properties of Fe2O3 nanoparticles embedded in hollows of periodic nanoporous silica.* Journal of Applied Physics, 2010. **108**(3): p. -.

40. Winkler, P.F., et al., *Magnetic-Moment of Proton in Bohr Magnetons.* Physical Review A, 1972. **5**(1): p. 83-&.

41. Maeda, H., et al., *Tumor vascular permeability and the EPR effect in macromolecular therapeutics: a review.* Journal of Controlled Release, 2000. **65**(1-2): p. 271-284.

42. Nicholls, P., *Introduction: the biology of the water molecule.* Cellular and Molecular Life Sciences, 2000. **57**(7): p. 987-992.

43. Liu, T., et al., *Bondlength alternation of nanoparticles Fe2O3 coated with organic surfactants probed by EXAFS.* Nanostructured Materials, 1999. **11**(8): p. 1329-1334.

44. Euclid, I. Todhunter, and R. Simson, *The Elements of Euclid*. 1933, London,: J. M. Dent & sons ltd.;. xviii p., 1 l.,.

45. Artmann, B., *Euclid : the creation of mathematics*. 1999, New York: Springer. xvi, 343 p.

46. Brass, P., W.O.J. Moser, and J. Pach, *Research problems in discrete geometry*. 2005, New York: Springer. xii, 499 p.